



ELSEVIER

Contents lists available at ScienceDirect

Bioorganic & Medicinal Chemistry

journal homepage: www.elsevier.com/locate/bmc

Broad assessment of bioactivity of a collection of spiroindane pyrrolidines through “cell painting”



Manvendra Singh^a, Nathan Garza^a, Zachary Pearson^a, Justin Douglas^{a,b}, Zarko Boskovic^{a,*}

^a Department of Medicinal Chemistry, University of Kansas, Lawrence, 66045 KS, United States

^b Nuclear Magnetic Resonance Laboratory, University of Kansas, Lawrence, 66045 KS, United States

ARTICLE INFO

Keywords:

Photochemistry
Biological activity
Complexity
Fingerprints

ABSTRACT

A collection of small molecules has been synthesized by composing photo-cycloaddition, C–H functionalization, and *N*-capping strategies. Multidimensional biological fingerprints of molecules comprising this collection have been recorded as changes in cell and organelle morphology. This untargeted, phenotypic approach allowed for a broad assessment of biological activity to be determined. Reproducibility and the magnitude of measured fingerprints revealed activity of several treatments. Reactive functional groups, such as imines, dominated the observed activity. Two non-reactive candidate compounds with distinct bioactivity fingerprints were identified, as well.

1. Introduction

Small organic molecules possess unique features that allow them both to probe and to modulate biological systems.¹ The structural features that inscribe particular biological activities into the small molecules are in general unknown, but the diversity of biologically active molecules is at least as broad as the range of biological activities observable at the organismal, cellular and biochemical levels combined. To find new lead compounds, as opposed to hits in a specific assay, the challenge for medicinal chemists is to reach new regions of chemical space and learn about the biological activities that may be provoked as quickly and efficiently as possible.² Both naturally-evolved and synthetically-created products suggest that the complexity of their structures plays an important role in endowing them with the potency and specificity required to reliably perturb intricate functions of the biological systems.^{3,4} Diverse chemical origins of molecules (i.e. the sequence of chemical reactions that gave rise to them, either through a biosynthetic gene cluster, or a combinatorial synthesis scheme) correlate best with the uniqueness of their protein-binding profiles.⁵ These two notions taken together charge chemists with creating a variety of reaction sequences that produce small molecules with complex structures. Image-based cell profiling techniques offer one way to assess quantitatively and reproducibly, multiple markers of the biological activity of a newly-synthesized small molecule.⁶ Perturbations induced by a small molecule lead to changes in cell morphology that can be captured by staining with fluorescent dyes, imaged microscopically,

and analyzed quantitatively to create a numerical “fingerprint” of a cell’s response.⁷ This process is called “cell painting.” Correlating the chemical-induced changes observed for a set of reference compounds having known but diverse biological activities generates a database that can be used to guide the screening of completely new compounds to uncover those whose “biological activity profiles” are similar, at least at the cellular level, to the reference compounds. These broad observations allow one to screen multiple new chemical entities for multiple, disparate, potential biological activities in one experiment. An outstanding attribute of many biologically-active natural products that is not always reflected among synthetic compounds is their stereochemical richness. To approximate this richness in the synthesis of completely new scaffolds, we have taken advantage of the high-energy intermediates involved in photochemical processes. Ultraviolet light infuses small molecules with enough energy to radically reconfigure their often flat, two-dimensional carbon skeletons.⁸ Many synthetically useful transformations have been achieved by gaining control of chemistry that follows the absorption of a photon.⁹ Complex and “unusual” scaffolds that are generated in this fashion can be further elaborated by the application of modern chemistry that relies on the activation of carbon-hydrogen bonds.¹⁰ Our overall synthetic strategy consists of combinations of four basic transformations: (1) photo-cycloaddition between phenylpyrroline and electron-poor terminal olefins; (2) electrophilic aromatic C–H functionalization with an activated thianthrene; (3) palladium-catalyzed C–C bond formation; (4) *N*-capping alkylation or carbamylation reactions.

* Corresponding author.

E-mail address: zarko@ku.edu (Z. Boskovic).

<https://doi.org/10.1016/j.bmc.2020.115547>

Received 13 March 2020; Received in revised form 23 April 2020; Accepted 2 May 2020

Available online 19 May 2020

0968-0896/ © 2020 Elsevier Ltd. All rights reserved.

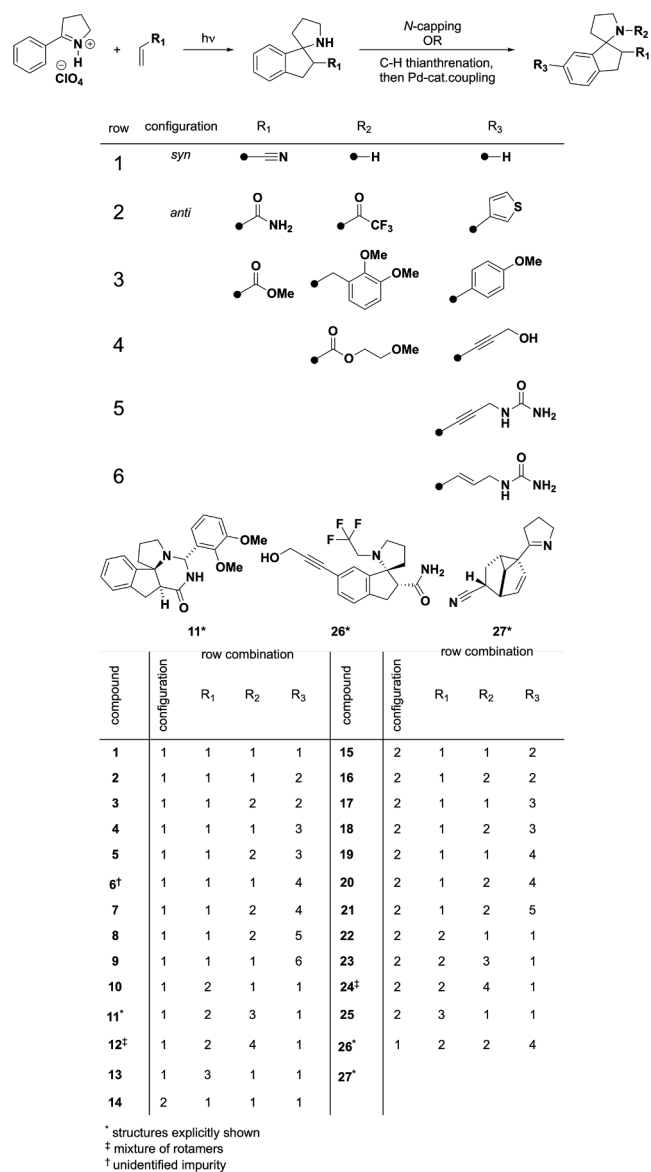


Fig. 1. Twenty-seven-member compound library. Structure of each compound (bottom table) can be obtained as a combination of rows from the top table. First column describes the relative configuration between pyrrolidine nitrogen and the group R₁, and columns 2, 3, and 4 specify the substitution of the spiroindane scaffold at the top of the figure.

To illustrate the complete concept outlined above, we describe herein a strategy for rapidly synthesizing a collection of 27 new compounds that contain a spirocyclic amine scaffold, together with the preliminary insights to the biological activities at the cellular level, vis-a-vis 13 selected reference compounds having diverse biological activities. Those that show interesting biological activities may serve as starting points for further elaboration for studying structure–activity relationships and for expanded biological testing. Multidimensional fingerprinting of the synthesized library of compounds led us to identify four bioactive compounds with different “cell painting” profiles compared to the reference set.

2. Materials and methods

2.1. Chemistry

A small library of 27 racemic compounds (Fig. 1) was synthesized from a single starting molecule – phenylpyrrolinium perchlorate. Six

core spiroindane scaffolds (three diastereomeric pairs) were generated in a photocycloaddition reaction between phenylpyrrolinium perchlorate and acrylonitrile (1 and 14), acrylamide (10 and 22), or methyl acrylate (13 and 25). This was achieved by irradiating 14 mM solutions of starting material in acetonitrile with a 500 W Hg-Xe lamp whose output was filtered with a band pass filter permissive to wavelengths in the range 255–305 nm. Diastereomers obtained in these photocycloadditions were separated by column chromatography. Further, site-selective C–H functionalization of the aromatic ring of aryl spiroindane scaffold was achieved by the introduction of tetrafluorothianthrene. Spiroindane pyrrolidine substrates were exposed to trifluoroacetylated tetrafluorothianthrene-S-oxide and tetrafluoroboric acid. The products were chromatographically isolated as tetrafluoroborate salts. Trifluoroacetyl groups that were introduced in thianthreneation reaction were removed with sodium borohydride in methanol to yield compounds 2, 4, 6, 9, 15, 17, 19, and 26. Compounds 2–5, and 15–18 were prepared from the corresponding thianthrenium salts and *p*-methoxyphenylboronic acid, catalyzed by tetrakis (triphenylphosphine) palladium(0) or bis(diphenylphosphino) ferrocene palladium(II) chloride (10–20 mol%), and basified with tribasic potassium phosphate. Similarly, compounds 6–9, 19–21, and 26 were prepared from thianthrenium salts and propargyl alcohol, or propargyl urea in reactions catalyzed by tetrakis (triphenylphosphine) palladium(0) at 10 mol%, in the presence of diisopropylamine as a base, and copper(I) iodide. Compounds 11 and 23 were prepared under reductive amination conditions with pyrrolidines and 2,3-dimethoxybenzaldehyde in the presence of sodium triacetoxyborohydride, whereas compounds 12 and 24 were prepared from the spirocyclic amine scaffold with 2-methoxyethyl chloroformate and triethylamine in dichloromethane. Complete description of the syntheses, isolation, and characterization of the compound collection can be found in the [Supporting Information document](#).

2.2. Cell painting

Culture: U-2 OS (ATCC, HTB-96) cells were cultured in T-75 flasks (Greiner, 658170) under McCoy's 5a medium (HIMedia, AT057), supplemented with 10% Fetal Bovine Serum (FBS) and 1% Penicillin/Streptomycin solution, and incubated at 37 °C in a 5% CO₂ atmosphere. Upon reaching 80% confluence, cells were washed, trypsinized (VWR, M143), and removed. Flasks were reseeded with one fifth of the cell count for each passage. All cell plates reported in this paper were composed of U-2 OS from incubation lengths of five or fewer passages. These optical-bottomed, 384 black well plates (Corning, 6569) were seeded with U-2 OS at a density of 1,000 cells per well and allowed to incubate for 24 h to ensure adherence. **Compound handling:** Compound plates (Thermo Scientific, AB-1056) were constructed using an initial aliquot of a 50 mM compound solution solubilized in DMSO. Each compound aliquot was then threefold serially diluted in DMSO to yield six concentrations ranging from 50 mM to 205 μM. This process was repeated for each of the twenty-seven test compounds and the starting phenylpyrrolinium perchlorate. Forty-one vehicle treatments were included in the plate design as DMSO containing wells with no added compound. Staurosporine diluted to 500 μM in DMSO was included on the plate as a positive control. A second plate composed of known toxic compounds was constructed using a maximum concentration on 10 mM, and was threefold serially diluted to a minimum concentration of 509 nM, except as noted in the Supplemental Material. This control plate also contained 190 wells filled with only DMSO to serve as vehicle treatment. **Compound treatment:** Subsequent to a 24 h incubation period, untreated cell plates and the compound plate were each fitted into a Library Copier and a sterile Multi-Blot Replicator (V&P Scientific) was used to transfer a 100 nL volume from each well of the 384 well compound plate into the culture media (50 μL) of a corresponding well on the 384 well cell plate. These cell plates were reintroduced to a 37 °C, 5% CO₂ atmosphere for the duration of the 24-h treatment period.

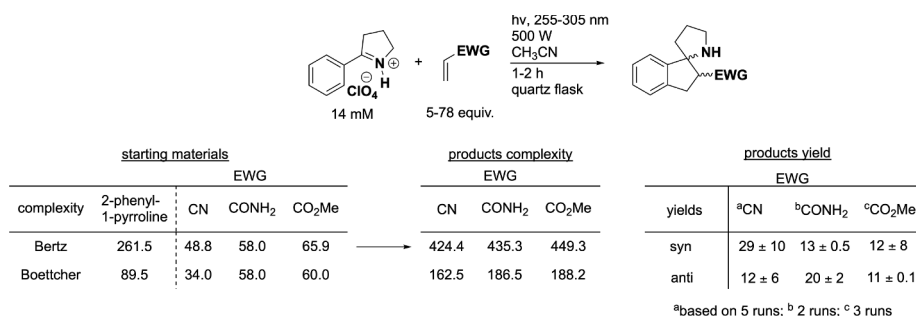


Fig. 2. Mariano photocycloaddition between flat phenylpyrrolinium perchlorate and electron-poor olefins produces spirocyclic scaffolds of significantly increased complexity.

Staining: Upon completion of the treatment period, cell plates had their media replaced with RPMI media (Sigma, R8755) without phenol red (10% FBS, 1% Penicillin/Streptomycin solution), containing 500 nM Mitotracker Deep Red (Thermo Fisher, M22426) in DMSO and 60 µg/mL Wheat Germ Agglutinin/Alexa Flour 594 (Thermo Fisher, W11262) in deionized water. The cell plates were incubated for an additional 30 min at 37 °C in 5% CO₂. The cells were then fixed in their wells with 4% formaldehyde (Electron Microscopy Sciences, 157110-S) for 20 min at room temperature, protected from light. Following a wash in Hank's Buffered Saline Solution (HBSS), cells were permeabilized with a 15 min incubation with a 0.1% solution of Triton X-100 (VWR, M143) in HBSS at room temperature, protected from light. After permeabilization, cells were washed in HBSS. The second staining solution composed of 1% BSA (VWR, 0332) in HBSS, 0.025 mL/mL Phalloidin/Alexa Flour 594 (Thermo Fisher, A12381), 100 µg/mL Concanavalin/Alexa Flour 488 (Thermo Fisher, 11252), 5 µg/mL Hoechst 33342 (Thermo Fisher, H3570), and 3 µM Syto 14 (Thermo Fisher, S7576) was then added and allowed to incubate for 30 min at room temperature, protected from light. A final HBSS wash concluded the staining process and the cell plates were sealed with aluminum sealing tape and imaged. Experiments were repeated 3 times with cells from different passages. **Imaging:** Sealed plates were imaged using an ImageXpress Micro XL microscope and MetaXpress image acquisition software. Five wavelength channels, DAPI, GFP, Cy3, Cy5, and TxRed, were used to capture fluorescent images of each well at 10 × magnification, and with 2 × 2 binning. Each well was divided into four quadrants in order to capture the entire well at the selected magnification. Whole plate imaging was preceded by an initial focusing step using the DAPI channel. Images were stored on a local hard drive to be analyzed by Cell Profiler.¹¹

2.3. Data analysis

Cell Profiler output comprises extracted feature values from 5 image sets for each of four sites of each of 384-wells of compound- or vehicle-treated cells. Features are initially measured per object (cell, nucleus, or cytoplasm) and can be averaged by Cell Profiler to give per-site values, that we averaged subsequently. We first calculated the average feature values for DMSO-treated cells (190 wells on the control plate, 41 on the test plate) together with the variability in these measurements, which was represented as the standard deviation of the measurements. We then subtracted the DMSO-derived averages from the treatment conditions and we divided this number with the standard deviation to obtain the Z-scaled value for each feature. From the Z-scaled values we computed the magnitudes of feature vectors by taking their norms, and we computed correlations between replicates, or between the active compounds (including controls) by taking the inner products of the appropriate feature vectors and dividing with the products of their lengths (cosine similarity). The magnitude of feature vectors is a measure of difference between the compound and vehicle treatments. The correlation between replicates or between the active compounds is a measure of similarity of those conditions.

3. Results & discussion

3.1. Synthesis of the compound collection

We used a photochemical reaction developed by Mariano¹² to prepare spiroindane pyrrolidine scaffolds in one step by pairing a single readily available starting material, 2-phenyl-1-pyrrolinium perchlorate,¹³ with 3 electron-deficient olefins – acrylonitrile, acrylamide, and methyl acrylate. Excitation of pyrrolinium salts is achieved by irradiation with ultraviolet light from a 500 W Hg-Xe lamp, filtered with a band pass filter (transmissive for wavelengths 255–305 nm), over 1 h in acetonitrile at 14 mM concentration. The fate of the phenylpyrrolinium excited state in the presence of electron-poor olefins is best explained by an initial [π ,2 + π ,2] arene-olefin cycloaddition to produce a bicyclic diene. Quaternary carbon-carbon bond migration (1,2-rearrangement) by cyclobutane ring expansion in concert with deprotonation generates the spirocyclic amine system and rearomatizes benzene. Alternatively, the mechanism may invoke the formation of a singlet biradical intermediate, followed by an electron-transferring oxidation of olefin (formation of a radical cation) and reduction of N-centered radical to amine.¹² Recombination of radicals, and elimination leads again to the final spirocyclic amine product. Regardless of these intriguing mechanistic underpinnings, the reaction reliably produces a chromatographically separable mixture of *syn*- and *anti*-benzospirocyclic amines (Fig. 2). Obtained NMR data matches the reported NMR of the *syn*- and *anti*-spiroamino nitriles and spiroamino esters.¹⁴ Relative configuration of spiroamino amides was determined by dehydrative conversion of primary amide to nitriles that we inadvertently accomplished¹⁵ during the thianthrenation reaction (in the presence of trifluoroacetic anhydride). All the secondary amines are most easily visualized with a ninhydrin stain upon resolving on a thin-layer chromatography plate.

Intuitive grasp of the increase in structural complexity provided by this transformation is confirmed by the two complexity descriptors which we used to measure it. Both Bertz¹⁶ and Böttcher¹⁷ complexity indices increase by about 30% in this reaction (sum of the complexity indices of starting material compared to the product complexity index). Qualitatively, exploration of the insufficiently studied chemical space of compounds containing spirocyclic amines¹⁸ provides additional motivation for the development of small collections featuring this structural motif. Hinting to the utility that photochemistry may hold as a method for generating structurally diverse compound collections, the photocycloaddition reaction with acrylonitrile afforded a novel, completely dearomatized 2,4-*meta*-cycloadduct, compound 27, in addition to *syn*- and *anti*-amino nitriles. We verified its structure through the X-ray diffraction pattern analysis (Fig. 3; CCDC: 1976540) and included it as part of the collection for bioactivity assessment. Diversification of the aromatic portion of the spirocyclic scaffolds necessitated that either a proper substituent is carried through the photochemical step, or that selective carbon-hydrogen functionalization protocol is implemented after the photo-cycloaddition. The effect of phenylpyrrolinium

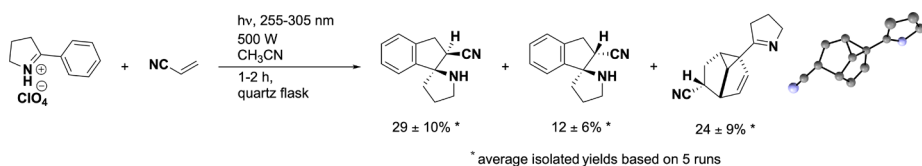


Fig. 3. Photochemical reactions produce complex molecules. Crystal structure of compound **27**, dihydrosemibullvalene derivative. CCDC: 1976540.

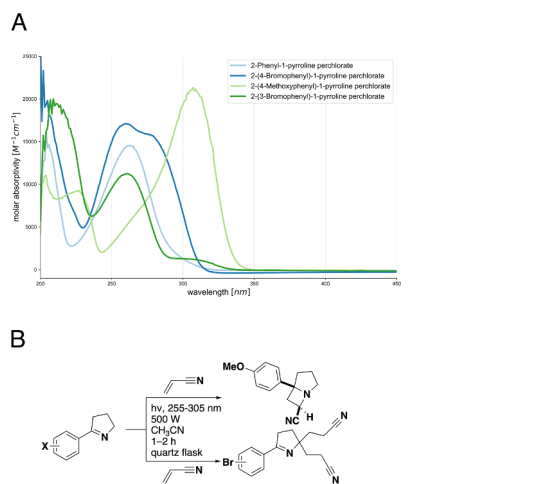


Fig. 4. (A) Substitution of phenylpyrrolidinium strongly impacts the electronic nature of the phenyl ring as evidenced by changes in the absorption spectra; (B) Tentatively assigned structures obtained from various substituted phenylpyrrolidinium perchlorates and acrylonitrile.

substitutions is apparent in the changes in absorption spectra in UV region of the spectrum (Fig. 4A), and these changes manifested themselves as different reactivity of substituted phenylpyrrolidinium salts in the photochemical reaction. For example, *p*-methoxy substituted phenylpyrrolidinium undergoes a $[\pi_2 + \pi_2]$ cycloaddition with the imine functional group instead of the benzene ring.¹² This leads to the formation of azetidine and no C–C bond migration during the rearomatization event. Bromo substituted substrates surprisingly undergo a radical conjugate addition to acrylonitrile from the 5-position of 1-pyrroline (Fig. 4B).

Strategically, in this diversity-oriented synthetic campaign, the sensitivity of the substrate towards substitution necessitated considering the carbon–hydrogen bond functionalization at a post-photochemistry stage to introduce groups at the aromatic portion of spiroindane pyrrolidines. The presence of four electronically similar C–H bonds called for a mild reagent for electrophilic aromatic substitution, such that it would be capable of distinguishing between minor differences in nucleophilicity of these positions. Reactivity and kinetics of thianthrene cation-radical perchlorate with aromatics have been explored by Shine in the 1970s.¹⁹ Those studies showed that electron-rich aromatics are preferred substrates and that the electrophilic aromatic substitution takes place *para* to the directing group. Ritter recently reported a modified version of this S_EAr reaction by employing tetrafluorothianthrene *S*-oxide and trifluoroacetic anhydride in the presence of tetrafluoroboric acid.²⁰ The thianthrene radical cation generated under these conditions reacts regioselectively with a wider variety of aromatic substrates compared to Shine's set-up. We used these conditions to introduce a chemical handle into *syn*- and *anti*-amino nitriles and to further elaborate these pseudo-halides through palladium-catalyzed C–C bond forming reactions, e.g. Sonogashira and Suzuki (Fig. 5). As expected, trifluoroacetic anhydride, used for the activation of *S*-oxide, rapidly reacts with free secondary amines in our substrates before the sluggish aromatic substitution reaction can take place. This necessitated a reductive removal of trifluoroacetamide with sodium borohydride, as methanolysis attempts were unsuccessful. In the context of initial diversification of the library through the variation of

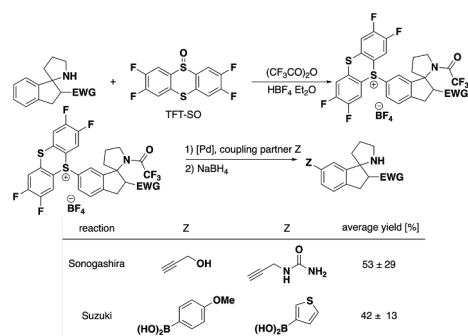


Fig. 5. Diversification of the aromatic portion of spiroindene pyrrolidine scaffolds has been accomplished through C–H functionalization. Regiochemistry of the substitution was determined from HMBC correlations from the aromatic singlet to the quaternary carbon.

electron-withdrawing groups on alkene partners in the Mariano photocycloaddition, this reductive step precluded the use of groups that can be reduced by sodium borohydride (e.g. esters, ketones). Interestingly, the attempted thianthrene reaction on primary amides, produced nitrile products through an eliminative process that follows *O*-acylation with trifluoroacetic anhydride, without the need for additional base common in these dehydrations.¹⁵

To achieve scaffold elaboration on the secondary amine, we relied on a well-precedented reductive amination with aromatic aldehydes,²¹ and the carbamate formation with a chloroformate (Fig. 6A). Employing these two conditions on spiroindane pyrrolidine amides furnished tertiary amines and carbamates, the latter existing at room temperature as a mixture of rotamers (Fig. 6B).²² In the NOE experiment, the selective irradiation of the characteristic methoxy peak of compound **12** at 3.47 ppm, produces a negative peak corresponding to the irradiated signal itself, as well as a peak at 3.12 ppm in the same phase. This confirms that signals are equilibrating at a rate faster than the NMR NOE relaxation.

The attempt at reductive amination of the *syn*-amino amide

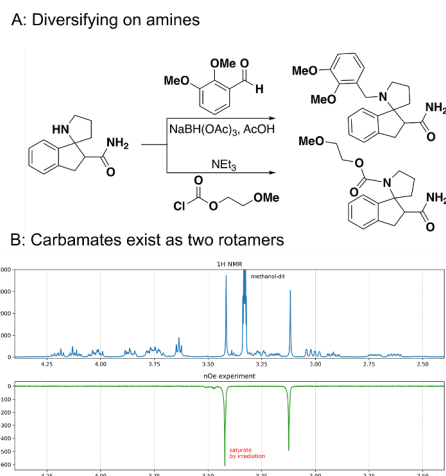


Fig. 6. Secondary amines were alkylated in reductive amination reaction or carbamylated with a chloroformate. Carbamates exist as two rotamers in approximately equal amounts.

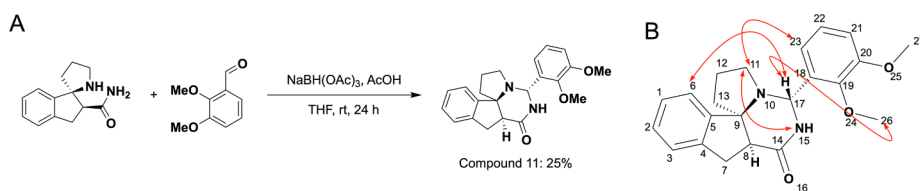


Fig. 7. (A) *Syn*-amino amide forms cyclic aminal under the reductive amination conditions; (B) Important NOE correlations for assignment of the aminal configuration.

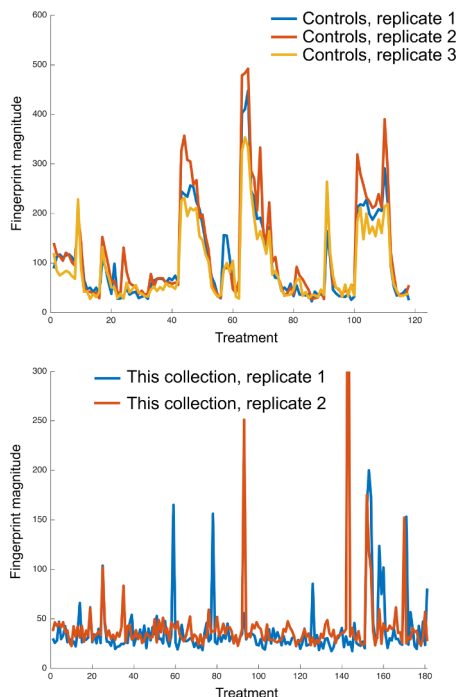


Fig. 8. Reproducibility of the “cell painting”-derived bioactivity fingerprints. Control compounds produce strong fingerprints (compare the y-axes), and measured features correlate well between replicates.

produced a stable pentacyclic aminal (compound **11**, Fig. 7A) that resisted reduction with sodium triacetoxyborohydride. Configuration assignment of the aminal carbon has been determined in NOESY experiment (Fig. 7B). *Ab initio* modeling suggests the *exo*-arrangement to be about 5.5 kcal/mol more stable than the *endo*-one. This cyclization was not observed for the *anti*-isomer, which further suggests that proximity of the amide nitrogen and transiently formed iminium is critical for cyclization.

The tangible outcome of the synthetic campaign described in previous paragraphs is a collection of small molecules in 5–20 mg quantities (Fig. 1) based around a common spiroindane pyrrolidine scaffold. Computed structural properties of the collection place it in a favorable property space for biological activity profiling (Supporting Information: Cheminformatics). The average molecular weight of the collection is 302.28 g/mol, AlogP²³ is 2.42, and the median number of hydrogen-bond donors and acceptors are 3 and 1, respectively. The mean polar surface area of molecules in the collection is 56.57 Å². A typical representative of the collection has one aromatic ring and one rotatable bond – both structural descriptors testifying to the relative rigidity of the molecules in this collection. Structural alerts triggered by the compounds in the collection are due to the presence of alkyne or ester functional groups.

3.2. Analysis of biological fingerprints

We embarked on the experiments described in this paper with a goal of tailoring the technique of “cell painting” to fit our needs for assessing our biological-assays-naïve compound collection. Our research group is

interested in understanding connection between structural complexity of small molecules and their biological activity. Against that backdrop, we designed a compound collection centered around spirocyclic scaffold of spiroindane pyrrolidines (vide supra). To quickly learn about the biological activity of molecules in this collection, we performed an experiment in which changes in cell morphology upon compound treatment are observed under a microscope after organelle-specific staining with fluorescent dyes (i.e. we performed a “cell painting” experiment).²⁴ We chose fast-growing U-2 OS cells for this assessment due to their exaggerated morphology, which lends itself to easily observable organellar staining. Performing these experiments in 384-well plates allowed us to test a range of compound concentrations (descending from 100 μM to 0.41 μM for test compounds) to ensure that we were not missing activities that are observable only at high or low concentrations.²⁵ These experiments can create a broad fingerprint of biological activity of newly-synthesized compounds. Similarity between fingerprints can indicate a shared mechanism of action and provide a clue about which targets or, more broadly, pathways are modulated by the action of the small molecule. While the power that multidimensional measurements bring to rapid assessment of biological activity of newly-synthesized compounds is undeniable, the obstacles to wider adoption of this approach are centered around (1) the reproducibility of weak fingerprints, (2) the assignment of actual phenotypic meaning of the measured changes, and (3) the uncertainty with respect to the granularity of such measurements.

Other research groups have started defining positive controls for this type of experiment, and we adopted 13 compounds to use as the benchmark measurements here, as well.^{5,24} Ten concentrations and 3 repeated treatments (biological replicates) with control compounds helped us establish a reliable, quantitative understanding about what constitutes a *bona fide* change in cell and organelle morphology that can be measured in this experiment (Fig. 8). In a departure from previous methods of cell painting analyses, we opted against averaging the replicates, instead defining the reproducibility of the fingerprint as an average correlation for each pair of replicates. This approach led us to discard one of the biological replicates for the newly-synthesized compounds as the correlation with other 2 experiments was low. Upon closer inspection, we learned that the cells grew to greater density in that condition – a fact that hints to one major source of “instability” of observed fingerprints. Overall, the reproducibility among the control compounds was higher than for test compounds. Cosine similarity between replicates 1 and 2 was 0.5731, between 2 and 3 it was 0.6428, and between 1 and 3 0.5907. The same measure for reproducibility of fingerprints of the test compounds is lower, 0.2189. This is expected from a collection where the majority of treatments causes no change in cell morphology compared to DMSO. As a general rule, the magnitude of the fingerprint (defined as the length of 1969-dimensional vector of Z-scaled features) correlates with its reproducibility (defined as the inner product between fingerprint vectors from different replicates). As can be seen in Fig. 9, values of fingerprint magnitude under 50 are very unlikely to reach level of reproducibility of 0.7. The same figure shows that even positive controls can have weak fingerprints, likely at low concentrations where the effects of these bioactive compounds do not manifest themselves as changes in organelle appearance.

There are three main applications for “cell painting” in the context of newly-synthesized compound collections: (1) determination of raw bioactivity, which can be defined as a significant and reproducible

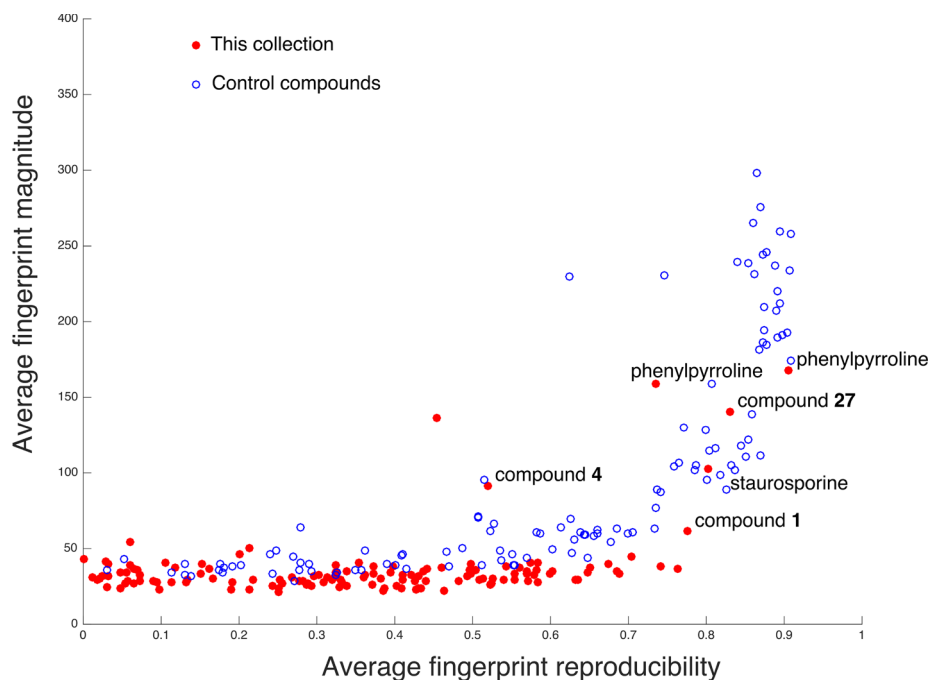


Fig. 9. Reproducibility and the magnitude of fingerprints allow for the identification of novel bioactive compounds from this compound collection. Each circle represents a “cell painting” fingerprint of one compound at a given concentration. Reproducibility shown on the abscissa is obtained by averaging correlations between replicates for each treatment. The magnitudes of fingerprints for each treatment were averaged and plotted on the ordinate. In addition to the chemically reactive phenylpyrroline and compound 27, compounds 1 and 4 produced moderately strong and reproducible changes in cell morphology.

Control compounds and active compounds from this collection grouped by fingerprints from **replicate 1**

Control compounds and active compounds from this collection grouped by fingerprints from **replicate 2**

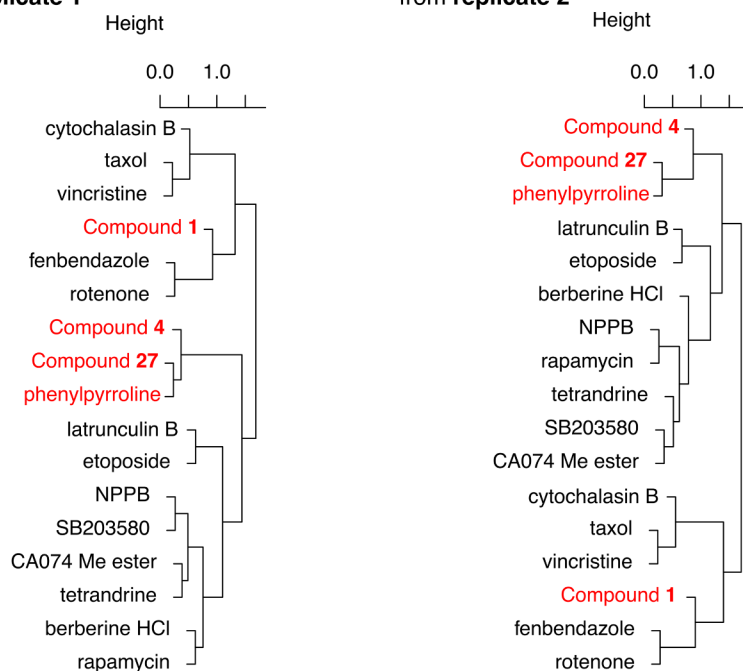


Fig. 10. Active compounds can be successfully grouped by cosine similarities of fingerprints quantifying the morphology changes they cause in cells.

change in appearance of organelles compared to DMSO treatment, (2) grouping of compounds based on similarity of their fingerprints which in a small collection would correspond to structure–activity relationships, and (3) assigning the mechanism-of-action of “active” treatments by similarity to the known bioactive compounds. This experiment revealed to us that the most active compound turned out to be the sole starting material for the collection synthesis! The precursor phenylpyrroline showed the strongest and most reproducible fingerprints in at least 2 concentrations (100 μ M and 33 μ M). A likely explanation for this activity is the reactive imine functional group. Strengthening

this explanation is the observed activity of compound 27, a dihydrosemibullvalene *meta*-cycloadduct, that also contains the same functional group. Previously reported imines and aziridines originating from different scaffolds were also common “active” compounds found in this type of experiment.²⁶ Based on the similarity of their fingerprints, phenylpyrroline and compounds 27 and 4 cluster together and away from any other control compound tested in this experiment (Fig. 10). Compounds 1 and 4 were the only non-imine containing compounds having moderately strong and reproducible fingerprints. These compounds are both *syn*-spirocyclic amino nitriles and have no

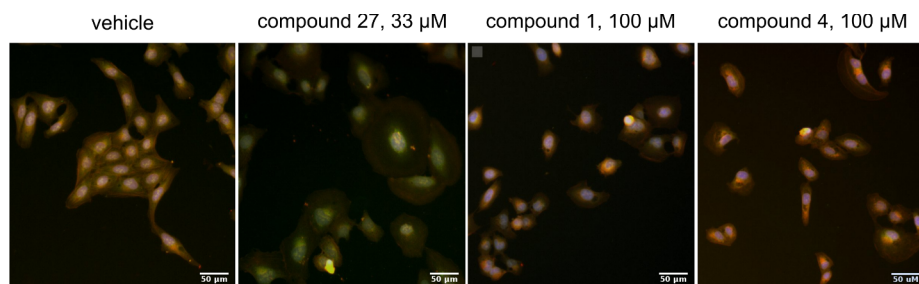


Fig. 11. Images of vehicle-treated cells and cells treated with compounds 1, 4, and 27. Differences in cell morphology are apparent even to a human eye. Composite image of all wavelengths is shown (blue: nucleus, green: ER, yellow: nucleoli, orange: Golgi and plasma membrane, red: mitochondria). (For interpretation of the references to colour in this figure legend, the reader is referred to the web version of this article.)

structural “red flags” associated with their structures (Supporting Information: Cheminformatics). Importantly, the corresponding diastereomers (compounds 14 and 17) are not active in this experiment, strengthening the case for a specific interaction that produces the activity. Based on the similarity of their fingerprints, compound 1 clusters with fenbendazole and rotenone, whereas compounds 4, 27, and phenylpyrroline all cluster together in a distinct clade (Fig. 10).

A qualitative interpretation of images of cells treated with compounds 1, 4, and 27 reveals drastic changes compared to vehicle treatment (Fig. 11). Each treatment was hallmarked by an increase in both mitochondrial and endoplasmic reticulum staining compared to that of vehicle-treated cells. Cytoplasmic swelling was commonly observed and severe membrane blebbing was abundant. This may indicate loss of the ability to control intracellular osmotic pressure. Nuclear fragmentation was clear and frequent. Furthermore, apoptotic bodies were numerous in the extracellular space for all the compounds that show increased toxicity. (See Supporting Information for complete data on toxicity of all control and test compounds.) Vehicle-treated cells are characterized by well-defined nuclei dotted with numerous nucleoli. Mitochondrial and ER stain intensities are balanced with that of cytoplasm stain. Cellular shape is defined by polygonal borders typical of U-2 OS cancer line. Imine-containing compound 27 (at 33 μM) produces a very strong ER and mitochondrial staining, and cells and nuclei are swollen. Compound 1 at 100 μM causes similar amplification of the mitochondrial staining. Membrane blebbing advanced with nuclear fragmentation, and misshapen cells are abundant with a few apoptotic bodies observed. Effects of compound 4 at 100 μM are similar to those of compound 1 with abnormally shaped cells, strong ER staining, and disappearance of numerous nucleoli present in normal U-2 OS cells.

One of the obstacles to the wider adoption of “cell painting” (vide supra) concerns the uncertainty with respect to the granularity of these fingerprints, i.e. what are the mechanisms that this technique can reliably distinguish? It seems apparent from the accumulated experience in this area that the compounds that target cytoskeleton will unsurprisingly produce the strongest fingerprints. In this study, we also observed that cytotoxic compounds seem to have strong fingerprints (they are obviously bioactive) and these fingerprints do not all seem to coalesce around common morphological changes. For instance, the imines (phenylpyrroline and compound 27) were cytotoxic, but this cytotoxicity produced a fingerprint different from the cytotoxicity of vincristine or taxol (Fig. 10). The mechanism of action of compounds 1 and 4 is difficult to precisely assign at this point, and is a topic of ongoing work in our laboratory. As a first step in this process, computational protein target prediction algorithm²⁷ suggested acetylcholine esterase and β -secretase as potential protein targets of these compounds.

4. Conclusions

We have described a synthetic chemistry strategy to prepare a collection of 27 molecules occupying new chemical space, and we generated their bioactivity fingerprints through “cell painting.” From these measurements we identified two compounds that could be classified as bioactive. This project demonstrated the feasibility of experimental

identification of starting points for the discovery of novel bioactive substances. Creative output of synthetic chemistry coupled with rapid insights that can be obtained from imaging cell populations treated with newly-synthesized compounds is a fertile ground for discovery of bioactive substances with novel mechanisms of action. Widespread adoption of this bioactivity assessment approach will benefit from a more standardized set of measured features. Unambiguous naming conventions would facilitate comparisons between fingerprints generated at different labs and originating from different experiments. Additionally, ascribing biological meaning to the observed changes would provide a more satisfying aspect to this biological annotation experiment. Connecting the compound structural features to the observed biological fingerprints has the potential to expedite structure–activity relationship studies and the identification of novel bioactive compounds.

Annotating the biological-assays-naïve compound collection with “cell painting” has provided us with the immediate experimental insights into the bioactivities of its members. We will use these insights to guide the improvements in synthetic chemistry to prepare the collection, and to define the exact mode of action of the active compounds.

5. Data statement

Raw images and Cell Profiler extracted features per-object are available upon request. Processed per-well files, analysis scripts, code to generate images, and compound.sdf files with annotated NMR shifts are available on the laboratory’s GitHub repository associated with this paper: https://github.com/boskovicgroup/spiroindane_pyrrolidines.

Declaration of Competing Interest

None.

Acknowledgments

We thank the University of Kansas New Faculty General Research Fund, General Research Fund, and Protein Structure–Function COBRE for financially supporting this project. We acknowledge Dr. Victor Day for X-ray diffraction experiments, and the NSF-MRI grant CHE-0923449 that was used to purchase the X-ray diffractometer and software used in this study. We thank Ms. Ankita Ramprasad, Ms. Annu Anna Thomas, and Mr. Matthew McCurry for their help with reproducing previously reported syntheses. We thank KU’s NMR core facilities for acquiring characterization data that made conclusions of this publication stronger. We are grateful to Prof. Robert Hanzlik for improving the quality of the manuscript, and to Prof. Patrick S. Mariano (University of New Mexico) for the helpful e-mail exchange regarding the structure of compound 27.

Appendix A. Supplementary material

Supplementary data associated with this article can be found, in the online version, at <https://doi.org/10.1016/j.bmc.2020.115547>.

References

- Schreiber SL. Chemical genetics resulting from a passion for synthetic organic chemistry. *Bioorg Med Chem*. 1998;6:1127–1152.
- Mignani S, Huber S, Tomas H, Rodrigues J, Majoral J-P. Compound high-quality criteria: a new vision to guide the development of drugs, current situation. *Drug Discov Today*. 2016;21:573–584.
- Selzer P, Roth H-J, Ertl P, Schuffenhauer A. Complex molecules: do they add value? *Curr Opin In Chem Biol*. 2005;9:310–316.
- Méndez-Lucio O, Medina-Franco JL. The many roles of molecular complexity in drug discovery. *Drug Discov Today*. 2017;22:120–126.
- Clemons PA, Bodycombe NE, Carrinski HA, et al. Small molecules of different origins have distinct distributions of structural complexity that correlate with protein-binding profiles. *Proc Nat Acad Sci*. 2010;107:18787–18792.
- Pahl A, Sievers S. The cell painting assay as a screening tool for the discovery of bioactivities in new chemical matter. *Syst Chem Biol, Springer*. 2019:115–126.
- Bray M-A, Singh S, Han H, et al. Cell painting, a high-content image-based assay for morphological profiling using multiplexed fluorescent dyes. *Nat Protoc*. 2016;11:1757.
- Karkas MD, Porco Jr JA, Stephenson CR. Photochemical approaches to complex chemotypes: applications in natural product synthesis. *Chem Rev*. 2016;116:9683–9747.
- Hoffmann N. Photochemical reactions of aromatic compounds and the concept of the photon as a traceless reagent. *Photochem Photobiol Sci*. 2012;11:1613–1641.
- Godula K, Sames D. C-H bond functionalization in complex organic synthesis. *Science*. 2006;312:67–72.
- Carpenter AE, Jones TR, Lamprecht MR, et al. Cellprofiler: image analysis software for identifying and quantifying cell phenotypes. *Genome Biol*. 2006;7:R100.
- Stavinoha JL, Mariano PS. Electron-transfer photochemistry of iminium salts. olefin photoadditions to 2-phenyl-1-pyrrolinium perchlorate. *J Am Chem Soc*. 1981;103:3136–3148.
- Sorgi KL, Maryanoff CA, McComsey DF, Maryanoff BE. N-vinylpyrrolidin-2-one as a 3-aminopropyl carbanion equivalent in the synthesis of substituted 1-pyrrolines: 2-phenyl-1-pyrroline. *Org Synth*. 2003;75:215.
- Mariano PS, Leone-Bay A. Photocycloadditions of electron poor olefins to 2-aryl-1-pyrrolinium salts. *Tetrahedron Lett*. 1980;21:4581–4584.
- Bruckner R. Carboxylic compounds, nitriles, and their interconversion. *Organ Mech: React Stereochem Synth*. 2010:321–338.
- Bertz SH. The first general index of molecular complexity. *J Am Chem Soc*. 1981;103:3599–3601.
- Böttcher T. An additive definition of molecular complexity. *J Chem Inf Model*. 2016;56:462–470.
- Müller G, Berkenbosch T, Benningshof JC, Stumpfe D, Bajorath J. Charting biologically relevant spirocyclic compound space. *Chem–A Eur J*. 2017;23:703–710.
- Shine HJ, Silber JJ. Ion radicals. xxii. reaction of thianthrenium perchlorate (C₁₂H₈S₂⁺ ClO₄⁻) with aromatics. *J Organ Chem*. 1971;36:2923–2926.
- Berger F, Plutschack MB, Riegger J, et al. Site-selective and versatile aromatic C–H functionalization by thianthrenation. *Nature*. 2019;567:223.
- Abdel-Magid AF, Carson KG, Harris BD, Maryanoff CA, Shah RD. Reductive amination of aldehydes and ketones with sodium triacetoxyborohydride. Studies on direct and indirect reductive amination procedures. *J Organ Chem*. 1996;61:3849–3862.
- Hu DX, Grice P, Ley SV. Rotamers or diastereomers? An overlooked NMR solution. *J Organ Chem*. 2012;77:5198–5202.
- Ghose AK, Viswanadhan VN, Wendoloski JJ. Prediction of hydrophobic (lipophilic) properties of small organic molecules using fragmental methods: an analysis of AlogP and ClogP methods. *J Phys Chem A*. 1998;102:3762–3772.
- Gustafsdottir SM, Ljosa V, Sokolnicki KL, et al. Multiplex cytological profiling assay to measure diverse cellular states, *PloS One* 8 (12).
- Perlman ZE, Slack MD, Feng Y, et al. Multidimensional drug profiling by automated microscopy. *Science*. 2004;306:1194–1198.
- Gerry CJ, Hua BK, Wawer MJ, et al. Real-time biological annotation of synthetic compounds. *J Am Chem Soc*. 2016;138:8920–8927.
- Mervin LH, Afzal AM, Drakakis G, et al. Target prediction utilising negative bioactivity data covering large chemical space. *J Cheminform*. 2015;7:1–16.